BBA - Molecular Basis of Disease 1865 (2019) 26–37

Contents lists available at ScienceDirect

BBA - Molecular Basis of Disease

journal homepage: www.elsevier.com/locate/bbadis

Phosphorylation of NHERF1 S279 and S301 differentially regulates breast cancer cell phenotype and metastatic organotropism

Maria Raffaella Greco[a,1], Emeline Bon[b,1], Rosa Rubino[a], Lorenzo Guerra[a], Manuel Bernabe-Garcia[c], Stefania Cannone[a], Maria-Luisa Cayuela[c], Loredana Ciaccia[a], Séverine Marionneau-Lambot[d], Thibauld Oullier[d], Gaëlle Fromont[b,e], Roseline Guibon[b,e], Sébastien Roger[b,f,*,2], Stephan Joel Reshkin[a,**,2], Rosa Angela Cardone[a,2]

[a] Department of Bioscience, Biotechnology and Biopharmaceutics, University of Bari, Italy
[b] Université de Tours, Inserm UMR1069, Nutrition, Croissance et Cancer, Tours, France
[c] Telomerase, Cancer and Aging Group, Research Unit, Department of Surgery, CIBERehd - University Hospital "Virgen de la Arrixaca", Murcia, Spain
[d] Cancéropôle du Grand Ouest, Nantes, France
[e] Centre Hospitalo-Universitaire de Tours, Tours, France
[f] Institut Universitaire de France, Paris, France

ARTICLE INFO

Keywords:
EBP50
SLC9A3R1
Invasion
Invadopodia
Metastases
Mesenchymal-vasculogenic transition
Vasculogenic mimicry

ABSTRACT

Metastatic cancer cells are highly plastic for the expression of different tumor phenotype hallmarks and organotropism. This plasticity is highly regulated but the dynamics of the signaling processes orchestrating the shift from one cell phenotype and metastatic organ pattern to another are still largely unknown. The scaffolding protein NHERF1 has been shown to regulate the expression of different neoplastic phenotypes through its PDZ domains, which forms the mechanistic basis for metastatic organotropism. This reprogramming activity was postulated to be dependent on its differential phosphorylation patterns. Here, we show that NHERF1 phosphorylation on S279/S301 dictates several tumor phenotypes such as *in vivo* invasion, NHE1-mediated matrix digestion, growth and vasculogenic mimicry. Remarkably, injecting mice with cells having differential NHERF1 expression and phosphorylation drove a shift from the predominantly lung colonization (WT NHERF1) to predominately bone colonization (double S279A/S301A mutant), indicating that NHERF1 phosphorylation also acts as a signaling switch in metastatic organotropism.

1. Introduction

Metastasis is the primary cause of death in cancer patients. Although some cancer cell properties involved in metastatic progression (such as local invasion, intravasation, and organ colonization) have been identified [1–3], the molecular mechanisms orchestrating both the determination of a particular malignant phenotype [4] and a specific metastatic organotropism [2] are still poorly understood. Signaling complexes are spatially and dynamically coordinated by scaffolding proteins, which allow for rapid phenotypical switches under microenvironment changes [5–7]. Changes in the scaffolding protein concentration, subcellular localization and/or interaction specificities can radically alter cell phenotype. This ability to reprogram cellular behavior forms the basis for cancer progression towards aggressive stages.

A number of studies have identified a central role for the scaffolding protein Na^+/H^+ Exchanger Regulatory Factor (NHERF1) in cancer. NHERF1 is upregulated in diverse cancers where its level of expression correlates with aggressive stage and poor prognosis [8–19]. NHERF1

Abbreviations: NHERF1, Na^+/H^+ Exchanger Regulatory Factor; NHE1, Na^+/H^+ Exchanger isoform 1; pHe, extracellular pH; pHi, intracellular pH; VM, vasculogenic mimicry; ECM, extracellular matrix; PDZ, Psd-95 (Post Synaptic Density Protein), DlgA (Drosophila Disc Large Tumor Suppressor) and ZO1 (Zonula Occludens-1 Protein); Dmut, S279A/S301A double mutant

* Correspondence to: S. Roger, Université de Tours, Inserm UMR1069, Nutrition, Croissance et Cancer, Faculté de Médecine de Tours, 10 Boulevard Tonnellé, 37032 Tours, France.
** Correspondence to: S.J. Reshkin, Department of Bioscience, Biotechnology and Biopharmaceutics, University of Bari, Via E. Orabona 4, 70125 Bari, Italy.
E-mail addresses: sebastien.roger@univ-tours.fr (S. Roger), stephanjoel.reshkin@uniba.it (S.J. Reshkin).
[1] These authors contributed equally as first authors to the work.
[2] These authors contributed equally as last authors to the work.

https://doi.org/10.1016/j.bbadis.2018.10.017
Received 15 May 2018; Received in revised form 21 September 2018; Accepted 11 October 2018
Available online 13 October 2018

contains two tandem PDZ domains and recruits membrane receptors and transporters, cytoplasmic cytoskeleton and signaling proteins into functional complexes that regulate cell processes that are relevant to cancer progression [20], including cell proliferation [12,16,17,21–24], survival [25], apoptosis [26], migration and invasion [8,27]. NHERF1 also controls growth factor receptor trafficking/function [12,23,28,29] and is involved in the inhibition of both growth and invasion induced by the EGFR inhibitors Gefitinib and Erlotinib [12,23].

In breast cancer cells, NHERF1 has been shown to organize molecular pathways, through its PDZ domains, that differentially determine the programs that regulate the expression of *in vitro* tumor phenotypes [30]. This PDZ domain-dependent reprogramming capacity of NHERF1 was postulated to be regulated *in vivo* by the differential phosphorylation of different serine residues [30]. Indeed, changes in phosphorylation state by cell- and context- specific kinases and phosphatases is one of the major mechanisms for regulating protein activities and functions, and NHERF1 is phosphorylated both constitutively and by (patho) physiological stimuli. The phosphorylation of serines 279 and 301 have been shown to regulate cell cycle [31,32], cell morphology, actin cytoskeleton organization and cell adherence to the extracellular matrix (ECM) [32] and the stability/half-life of NHERF1 itself [33].

In this study, we stably transfected the highly invasive, triple-negative (ER-, PR-, HER2-), human breast cancer cell line MDA-MB-231 with wild-type (WT) NHERF1, with NHERF1 mutated from serine to alanine such that they could no longer be phosphorylated in serine 279 (S279A), in serine 301 (S301A) or in either (S279A/S301A double mutant, Dmuts). We investigated the contribution of these residues of NHERF1 to cancer cell phenotype and invasion *in vitro* and in tumor growth and metastasis *in vivo*. Our results indicate that the NHERF1 phosphorylation state differentially controls (*i*) NHE1 activity and invadopodial-dependent ECM degradation, (*ii*) vasculogenic mimicry (VM) and the angiogenic secretome, (*iii*) soft-agar and 3D growth and (iv) the metastatic organotropism of cancer cells. We conclude that the possibility to phosphorylate the two serines separately or together permits the cell to very finely tune its phenotypic behavior and eventual metastatic organotropism.

2. Materials and methods

2.1. Reagents

Matrigel™ (Growth Factor Reduced) was from BD Bioscience. pH-sensitive (BCECF-AM, 2′,7′-bis-(2-carboxyethyl)-5-(and-6)-carboxyfluorescein), and all fluorogenic or fluorescent probes were from Molecular Probes. Primary antibodies: monoclonal anti-NHE1 (4E9, Abcam) for Western Blotting and polyclonal anti-NHE1 (Alpha Diagnostic) for immunocytochmistry, monoclonal anti-cortactin (4F1, Millipore), polyclonal anti-MMP2 (Cell Signaling), PTEN (A2B1) antibody (sc-7974) was from Santa Cruz, active (cleaved) caspase 3 antibody was from Bio Vision (3015) and mouse monoclonal antibody against actin was from Sigma. His-tag, p-AKT, AKT, p-ERK1/2 and ERK1/2 antibodies were all from Cell Signaling Technology. Rhodamine B, isothiocyanate, mixed isomers (TRITC) was purchased from Sigma. Secondary antibodies: anti-mouse (Sigma) and anti-rabbit (Cell Signaling) HRP-conjugated antibodies, goat anti-mouse and anti-rabbit AlexaFluor568, donkey anti-mouse AlexaFluor647 (Molecular Probes). The P4G11 antibody for β1-integrin stimulation was from Santa Cruz Biotechnology (sc-18845).

2.2. Cells and establishment of stable NHERF1 mutants

The human breast cancer cell line MDA-MB-231-Luc (expressing luciferase gene) was grown as described [8]. Cells were transfected with FuGene6 transfection reagent (Roche Molecular Biochemicals, USA) and 3 μg of DNA construct, according to the manufacturers protocol. Expression vectors for NHERF1-WT and NHERF1 mutated in the S279, S301 or S279/S301 to alanine were developed as described [34]. The transfected MDA-MB-231 cells were selected and maintained in complete medium containing 500 μg/ml Hygromycin B (Calbiochem, Germany). Clones were selected that had similar His-Tag expressions and that also had similar increased levels of NHERF1 expression compared to pcDNA stably transfected cells. When multiple clones had these similar levels of expression, we then tested them for anchorage-independent growth, invasion and vasculogenic mimicry levels. Supplemental Fig. 1 displays a representative Western Blot showing NHERF1, His-Tag and β-actin levels for the pcDNA and stable cell lines expressing the WT and various mutant clones.

2.3. ECM digestion using in situ zymography

Cells were seeded onto a layer of Matrigel™ (final concentration of 4 mg/ml) containing quenched DQ-Green BSA or DQ-red BSA, mixed to a final concentration of 30 μg/ml, on 12 mm round glass coverslips. 30,000 cells/coverslip were seeded onto the polymerized matrix and grown for 6, 8 and 24 h, then fixed with paraformaldehyde 3.7% in PBS. Invadopodia-dependent ECM digestion was evaluated microscopically. Focal proteolysis produces fluorescence within a black background which is used both to quantitatively measure proteolytic activity levels and in co-localization analysis. Cells were imaged for F-actin (phalloidin-AlexaFluor594 TRITC, SIGMA) and quantification of ECM degradation was done by counting degradation spots in 10 fields of view (40× objective) in 3 separate experiments for each cell line. The degradation area was determined by using ImageJ 1.41 software and normalized for the number of cells positive for focal degradation. ECM degradation was calculated as total focal digestive activity of 100 cells.

2.4. Measurement of intracellular pH (pHi) and extracellular pH (pHe)

Cells were incubated for 30 min at 37 °C in Hank's medium containing 2 μM BCECF-AM (λexc 503/440 nm; λem 530 nm). Excess dye was removed by rinsing the cells twice with PSS. Changes in intracellular pH (pHi) were measured and NHE1 activity calculated as H^+ efflux as previously described [4,35,36].

2.5. Measurement of proteolysis-driven extracellular pHe in the invadopodia

The pH of extracellular proteolysis areas was measured by fluorescence ratio imaging of unquenched fluorescein-conjugated gelatin DQ (FITC)-gelatin, that had been liberated by proteolysis of the ECM in which it was dissolved, as previously described [37]. Matrigel™ (4 mg/ml) containing 30 μg/ml of DQ-FITC-gelatin was coated onto confocal culture dishes (WillCo Wells BV, Amsterdam, Netherlands). 10^5 cells/dish were seeded 12 h before the experiment. Areas of digested ECM were imaged on a Nikon Eclipse TE2000S epifluorescence microscope equipped with a MicroMax 512BFT CCD camera (Princeton Instruments, NJ) using a Nikon lamp shutter with a mercury short arc photo optic HBO 103 W/2 lamp for excitation (OSRAM GmbH, Augsburg, Germany) and a 40× Nikon S-Fluor oil objective. Images were acquired with 490 nm (pH sensitive) and 440 nm (isobestic pH insensitive) excitation wavelength filters, using a 535 nm emission filter and analyses were performed with the MetaFluor® 4.6r9 software (Universal Imaging Corp.). Digested areas were selected and after signal stabilization (to determine the steady state ratio value), an extracellular alkalinization was produced by perfusing the cell layer with a Ringer solution (in mM: 140 NaCl, 5 KCl, 20 HEPES, 10 D-Glucose, 0.1 $CaCl_2$, and 1 $MgCl_2$) at pH 7.4 in which the fluid level of the dish was maintained by needle aspiration and extracellular pH (pHe) was followed over time. After a

lag time (4 to 6 min), cells began to re-acidify the areas of digested ECM and the initial rate of acidification was determined by linear regression analysis of the first 15 points taken at 4 s intervals after the re-equilibrium of the focal zones at pHe 7.4. The entire process was repeated to determine its reproducibility. *In situ* calibration curves were obtained by perfusing the cells with ringer solutions at different pH (6.2; 6.8; 7.2; 7.4; 7.8). At the end of the experiment, the dish was incubated with a ringer containing 0.5 mg/ml of crystal violet to quench all external fluorescence [38]. The background ratio in each analyzed area was subtracted.

2.6. In vitro invasion assays

In vitro cellular invasion was measured as the ability to traverse an 8-μm polycarbonate membrane coated with 5 μg of Matrigel™ as described previously [30]. For 3D evasion assay, 7.5×10^3 cells were included in serum-free Matrigel™ drops and incubated for 24 h in complete medium [30].

2.7. Colony formation in soft agar assays

The ability to grow in an anchorage-independent way was measured by the formation of colonies on soft agar. The base layer was prepared with DMEM:0.5% low melting temperature agarose (SeaPlaque, FMC BioProducts, Rockland, Maine). The feed layer was then prepared by resuspending 2×10^4 cells in DMEM:0.25% low melting temperature agarose in the presence of *hygromycin* B and pouring onto the previously prepared base layer (1/2 of the volume of the lower layer). Culture medium was changed every 2 days and colonies counted after 21 days. Diameter of produced colonies was measured.

2.8. In vitro 3D vasculogenic mimicry network formation assays

Unpolymerized growth factor-reduced Matrigel™ diluted to 7 mg/ml in serum-free medium (DMEM) was mixed with 10^4 cells and plated on dishes containing 22 mm glass coverslips. Dishes were carefully inverted for 30 min at 37 °C to allow Matrigel™ drops to polymerize and, subsequently, complete DMEM plus Hygromycin was added to each dish. After 5 days incubation, cell growth and organization were observed through an inverted phase-contrast light microscope (TE200, Nikon, NY, USA). Fluorescent staining of cord networks in whole-mount gels and subsequent reconstruction of vessel-like structures in 3D Matrigel™ were performed by fixing the Matrigel™ drops with 4% PFA (paraformaldehyde) for 20 min at RT. After washing with PBS, drops were subsequently incubated at RT for 30 min with PBS containing 0.5% Oregon Green® 488 DHPE, and washed with PBS.

2.9. Angiogenesis array

1.5×10^5 cells/well were seeded in 24-well cell culture plates. Medium was changed every 3 days. When reaching approximately 80% confluence, cells were incubated with 1 ml of DMEM without FBS, growth factors or antibiotics for 30 h. Conditioned media (CM) were collected, centrifuged and the supernatants were collected in new tubes and kept on ice. Each sample was prepared to 40 μg protein in a final volume of 1.5 ml. The 'Human Angiogenesis Array' Kit (R&D systems, Minneapolis, USA) was used for the detection of proteins associated with angiogenesis, according to manufacturer instructions.

2.10. Zebrafish invasion assays

The colonization of Zebrafish (*Danio rerio*) embryos by human cancer cells was performed as previously described [39]. This was approved by the Bioethical Committee of the University Hospital Virgen de la Arrixaca (Spain). Briefly, breast cancer cells were trypsinized, washed and stained with fluorescent CM-Dil (Vibrant, Invitrogen). 50–100 labelled cells were injected into the yolk sac of dechorionated zebrafish embryos. Fishes with fluorescently-labelled cells appearing outside the implantation area at 2 h post-injection were excluded from further analysis. All other fishes were incubated at 35 °C for 48 h and analyzed with a SteReo Lumar V12 stereomicroscope equipped with an AxioCam MR5 camera (Carl Zeiss). The evaluation criteria for embryos being invaded by human cancer cells was the presence of > 3 cells outside of the yolk sac.

2.11. In vivo mouse tumor model

All animals were bred and housed at the *In vivo* platform of the Cancéropôle Grand Ouest at Inserm U892 (Nantes, France) under the animal care license n° 44278. The project was approved by the French national ethical committee (ref n°00085.01). 2×10^6 MDA-MB-231-Luc-derived cells (in 100 μl PBS) were injected into the lateral tail vein of non-anaesthetized 6-week-old female NMRI Nude Mice (Charles River laboratories, France), as previously described [36]. BLI measurements were performed within 15 min after D-luciferin intraperitoneal injection (150 mg/kg). Photons were counted with a μimageur™ (BIOSPACE Lab) and expressed in counts per minute (cpm).

2.12. Statistical analyses

Statistical analyses on immunohistochemistry staining were performed using the Yate's chi-squared test using the online interactive software Quantsy (http://quantpsy.org). Data were displayed as mean ± standard error of the mean (SEM) (n = sample size) and were analyzed using parametric statistical tests (Student's *t*-test, or ANOVA) when they were following a normal distribution and equal variances. Alternatively, data were displayed as box plots indicating the first quartile, the median, and the third quartile, and squares for comparison of means. In these cases, adequate non-parametric statistical tests were used (Mann-Whitney rank sum tests, Dunn's tests, ANOVA on ranks). Statistical analyses were performed using SigmaStat 3.0 software (Systat software Inc.) and statistical significance is indicated as: *, $p < 0.05$; **, $p < 0.01$ and ***, $p < 0.001$. ns stands for not statistically different.

3. Results

3.1. In vitro and in vivo cancer cell invasiveness are controlled by phosphorylable residues S279 and S301 of NHERF1

Activation of the β1 integrin pathway is a critical pro-invasive signal that promotes invadopodial activity [40,41]. An unidentified phosphorylated form of NHERF1 takes part in the β1 integrin-dependent regulation of invadopodia formation and proteolytic function [42]. However, the potential involvement of phosphorylable S279 and S301 residues in NHERF1 in modulating cancer invasion is still unknown. Supplementary Fig. 2A shows the effect on NHERF1 phosphorylation levels of alanine substitution for serine in S279 and S301, either separately (S279A or S301A) or together (S279A/S301A double mutant, Dmut) in the absence and presence of β1 integrin activation with the integrin β1 activating antibody P4G11 (5 μg/ml). While little effect was observed on the total expression of NHERF1, these substitutions reduced both the levels and the molecular weight of the phosphorylated bands, suggesting that S279 and S301 can be phosphorylated.

The role of S279 and S301 of NHERF1 in MDA-MB-231 cell invasion, using the three different cell clones expressing NHERF1

(phosphorylation-dead) mutants, was first analyzed in Matrigel™-based invasion assays (Fig. 1A). In line with previously reported results [30], the overexpression of WT-NHERF1 significantly increased invasion (+152.9 ± 12%, n = 4, $p < 0.01$) and the mutation of S279 and S301 into non-phosphorylable alanine residues, either separately or together (Dmuts), completely abolished the invasive capacity attributed to NHERF1 overexpression. We then characterized the role of S279 and S301 of NHERF1 in three-dimensional evasion assay, when cancer cells were entrapped in Matrigel™. We found that MDA-MB-231 cells overexpressing WT-NHERF1 exhibited a more invasive phenotype than control cells (pcDNA), had a higher escape index (+ 161.9 ± 15%, n = 3, $p < 0.01$), while all cell clones expressing mutant NHERF1

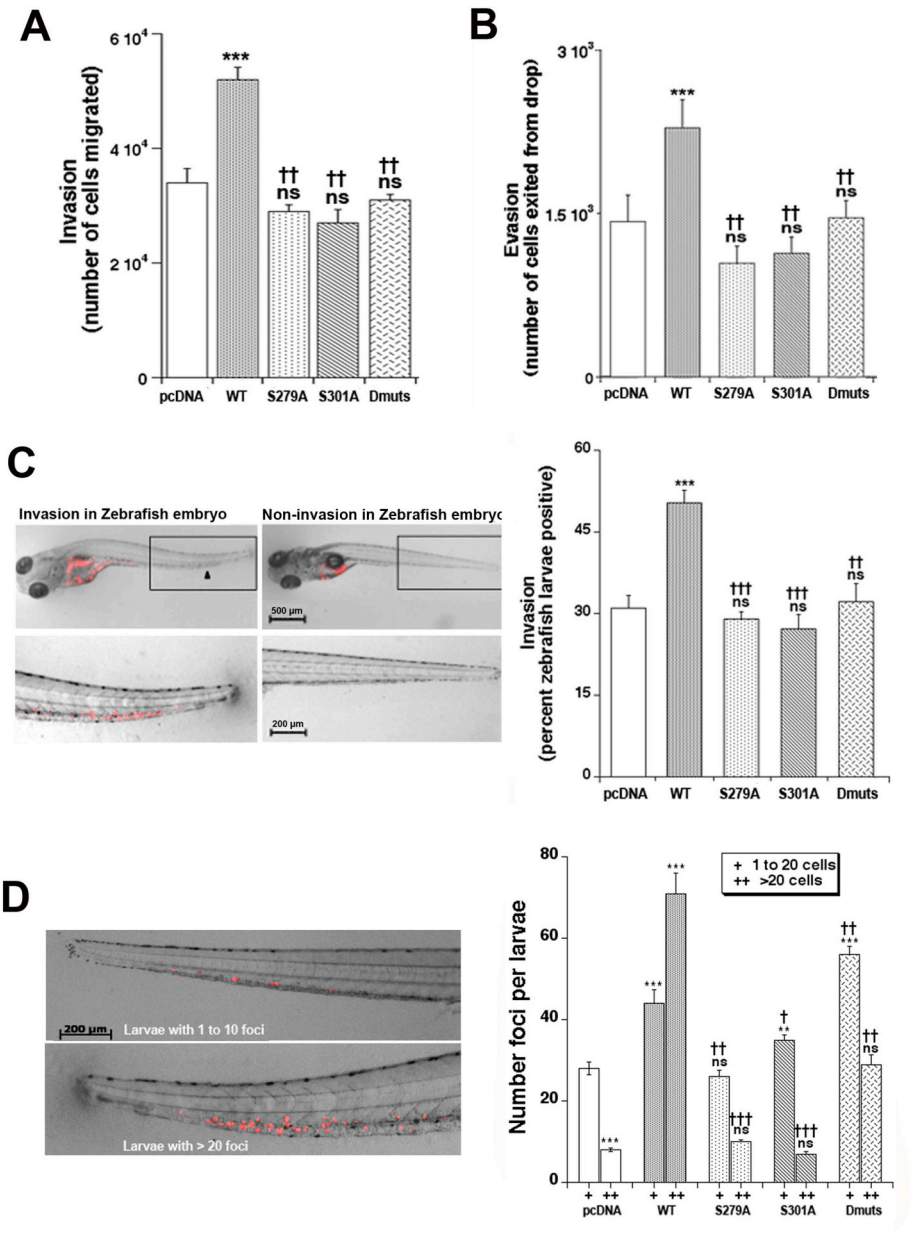

Fig. 1. S279 and S301 of NHERF1 regulate cancer cell invasion and invadopodia dynamics.

(A) MDA-MB-231-Luc-derived clones to invade were analyzed in Boyden chambers as described in Material and Methods. Data are mean ± SEM, n = 5 in triplicate. (B) The ability of the indicated MDA-MB-231 clones to evade from a Matrigel drop incubated at 37 °C for 6 days was analyzed as described in Materials and methods. Data are mean ± SEM, n = 5 in triplicate. Representative microphotographs of Matrigel evasion assays are presented in Supplemental Fig. 1B. (C) Left panel: representative images of zebrafish embryos injected in the yolk sac with MDA-MB-231-Luc–derived cells stained with the vital fluorescent tracker CM-Dil and showing sites of invasion into the tail; bar = 500 µM. A magnification of the highlighted region containing human cancer cells (red) invading the tail of the embryo is shown below each image, bar = 200 µM. Right panel: percent of the zebrafish embryos positive for invasion. Data are mean ± SEM, n = 5 in triplicate. (D) Left panel: representative images of different numbers of invaded cells in the tails of zebrafish embryos injected in the yolk sac with MDA-MB-231-Luc cells stained with the vital fluorescent tracker, CM-Dil; bar = 200 µM. Right panel: Percent of the zebrafish embryos positive for invasion for each of the indicated MDA-MB-231-Luc clones separated into two classes, depending on the number of invaded cells (< 20 cells; > 20 cells). Data are mean ± SEM, n = 5. (E) Invadopodial-dependent proteolysis of the ECM measured by an *in vitro* fluorescent-Matrigel degradation assay as described in Materials and methods. Cells were seeded on coverslips coated with Matrigel (4 mg/ml) and BSA-BODIPY (30 µg/ml) and incubated at 37 °C for 24 h. Quantification of invadopodia function (Invadopodia ECM Digestion) calculated as total focal digestive activity of 100 cells; mean ± SEM, n = 4.

For all histograms, *$p < 0.05$; **$p < 01$; ***$p < 0.001$ compared to pcDNA and ††$p < 0.01$; †††$p < 0.001$ compared to the WT clone.

remained entrapped in the Matrigel™ (Fig. 1B), under both the stimulation or not of the β1-integrin pathway (Supplementary Fig. 2B). In line with these invasion data, the WT-NHERF1 cells exhibited a more elongated cell morphology than the pcDNA cells and all cell clones expressing mutant NHERF1 had a more rounded shape (data not shown). We also assessed *in vivo* cancer cell invasiveness by employing a Zebrafish (*Danio rerio*) embryo model (Fig. 1C–D). When injected into the yolk sac, WT-NHERF1 overexpressing cells invaded organs of a higher percentage of larvae (Fig. 1C) and positive larvae also displayed higher numbers of invaded cancer cells compared to the control condition (pcDNA) (Fig. 1D). In comparison, all NHERF1 mutant cell lines had both a reduced percentage of positive larvae, and reduced numbers of invaded cells in the positive larvae. These data indicate that phosphorylated S279 and S301 confer the invasive advantage attributed to NHERF1 both *in vitro* and *in vivo*.

Proteolytic degradation of ECM is one of the key steps of cancer invasion [43] and highly invasive cancer cells display focalized protease-dependent proteolytic protrusive structures called invadopodia [44–46]. We have previously shown that overexpression of WT-NHERF1 increases breast cancer invadopodia proteolytic activity through its PDZ2 domain [30] and that a phosphorylated form of NHERF1 binds to a protein-lipid-protein complex in the invadopodia [42]. We, therefore, examined the distribution of invadopodia and their ECM focal proteolytic activity by confocal fluorescent microscopy of cells cultured on Matrigel™ containing quenched DQ-Green-labelled BSA-BODIPY [37]. The total invadopodia-dependent focal digestive activity was quantified by scoring the cells for the Invadopodial Index as defined in Materials and methods (Fig. 1E). Overexpression of WT-NHERF1 greatly increased invadopodia-dependent ECM digestion ($+186 \pm 8\%$, $n = 4$, $p < 0.001$ compared to pcDNA cells) while the over-expression of the S279A, S301A or S279A/S301A mutants was ineffective, suggesting that also invadopodial activity is equally controlled by the phosphorylation of NHERF1 at S279 and S301. Similar results were obtained under β1 integrin stimulation (Supplemental Fig. 2C–E).

Invadopodia formation and focal ECM proteolysis are known to depend on the Na^+/H^+ exchanger isoform 1 (NHE1) which drives extracellular acidification at the invadopodia [37,47–49]. Therefore, we measured the extracellular pH (pHe) and NHE1 activity at the invadopodia using Matrigel™ containing DQ(FITC)-gelatin as fluorogenic substrate of proteases in which the FITC released is pH-sensitive [38,50] (Fig. 2A). This method permits an analysis of pHe specifically at the invadopodia (Fig. 2B–C). An increased acidification of pHe was observed at the invadopodia stimulated by the β1 integrin activating antibody P4G11 (5 μg/ml) and was prevented by the specific NHE1 inhibitor HOE642 (1 μM) (Fig. 2D, Supplemental Fig. 2F). The overexpression of WT-NHERF1 potentiated invadopodial NHE1 activity ($+214 \pm 12\%$, $n = 8$, $p < 0.001$) while the overexpression of the S279A, S301A or Dmuts, completely abrogated this stimulation (Fig. 2E).

3.2. S301 of NHERF1 negatively regulates anchorage-independent colony and 3D spheroid growth

The ability of cancer cells to grow in an anchorage-independent manner and to form colonies in semi-solid media or on ultra-low adhesion plates is often regarded as one of the hallmarks of tumorigenicity and metastatic potential [51]. In soft agar matrix (Fig. 3A), control pcDNA cells formed numerous large colonies (> 100 μm diameter) while WT-NHERF1 cells mostly developed microcolonies (< 50 μm diameter). This suggests, as already proposed [30], that WT-NHERF1 overexpression reduces anchorage-independent growth of cancer cells. Interestingly, cells overexpressing the NHERF1 mutant S279A residue formed significantly smaller colonies than pcDNA that were slightly but significantly larger than the WT-NHERF1 cells, while cells expressing the S301A mutant formed colonies comparable to those of pcDNA cells. Dmuts cells formed intermediate-sized colonies to the S279A and S301A (Fig. 3A, right panel).

In ultra-low adhesion wells cells grew as single spheroids, whose increase in growth and change in morphology were analyzed after 7 days by both MTT assay and microscopy analyses (Fig. 3B). Control pcDNA clones formed round spheroids and the overexpression of WT-NHERF1 significantly reduced their growth. The growth of the mutant clones in low-adhesion wells closely followed that observed in soft agar: the S279A clone grew slowest, the S301A clone was the fastest, and the Dmuts clone grew at a slightly lower rate than the S301A clone (Fig. 3B, right panel).

Altogether, these data suggest that NHERF1 overexpression prevents both anchorage-independent and 3D spheroid-growth growth primarily *via* the phosphorylation of S301 and to a smaller extend to the phosphorylation of S279. NHERF1 has been shown to regulate survival through the PTEN-dependent inhibition of PI3K-phospho-AKT-mediated signals [25], proliferation through the ERK pathway [12,26,29,30,52–55] and increased apoptosis due to WT NHERF1 overexpression mediated by the suppression of ERK [26]. To verify if indeed S279 and S301 of NHERF1 impact survival and proliferation by altering PTEN-PI3K-AKT and ERK signaling, we analyzed by Western Blotting the level of PTEN and the phosphorylation status of AKT and ERK1/2 in pcDNA cells, NHERF1-WT cells and the phospho-dead mutant clones (Fig. 3C). Indeed, NHERF1-WT overexpressing cells increased PTEN expression compared to pcDNA cells and this required S279 and S301 as all phospho-dead-mutant cells (S279A, S301A and the double mutated, Dmuts) had lower levels of PTEN than the WT cells. In line with these data, WT-NHERF1 overexpressing cells showed a reduced level of p-AKT compared to pcDNA cells, while the level of p-AKT was progressively increased in S279A, S301 and Dmuts cells. Accordingly, NHERF1-WT overexpressing cells had a greatly reduced p-ERK1/2 with respect to pcDNAcells and this phosphorylation was restored in S279, S301 and Dmuts cells. We also found that WT-NHERF1 cells had increased active Caspase 3 expression respect to pcDNA cells and this increase required NHERF1 phosphorylated on both S279 and especially S301 as S279A cells, S301A cells and Dmuts cells had less active Caspase 3 in comparison to WT cells. These results confirm that NHERF1 growth-suppression function requires the phosphorylation of S279 and S301 to suppress both the PTEN/AKT-mediated survival and the p-ERK1/2 driven proliferation pathways and also increase Caspase 3-mediated death.

There is now clear evidence that NHE1-driven alkalinization of intracellular pH is an important mechanism driving increased cancer growth [56–58]. This paradigm was supported here since, in 3D non-adhesive growth conditions, NHE1-dependent H^+ efflux activity was strongly reduced in WT-NHERF1 cells and increased stepwise from the S279A mutant to the S301A mutant and finally to the Dmuts (Fig. 3D).

3.3. S279 and S301 are critical for NHERF1-dependent vasculogenic mimicry and secretion of pro-angiogenic factors

When grown embedded in growth factor-reduced Matrigel™, without added serum, some aggressive cancer cells, such as MDA-MB-231, are able to trans-differentiate to form vascular-like networks (vasculogenic mimicry, VM) [59]. This phenotype was increased by a dominant-negative mutation in the binding motif of the NHERF1-PDZ2 domain, the HRF2 mutation, and was associated with increased bone metastasis [30]. Therefore, we next analyzed the innate vasculogenic-like ability of the different NHERF1 clones (Fig. 4A). Control cells (pcDNA) generated a complex irregular 3D vascular-like tubular network emerging from multicentric cellular nodes, to delimit completely

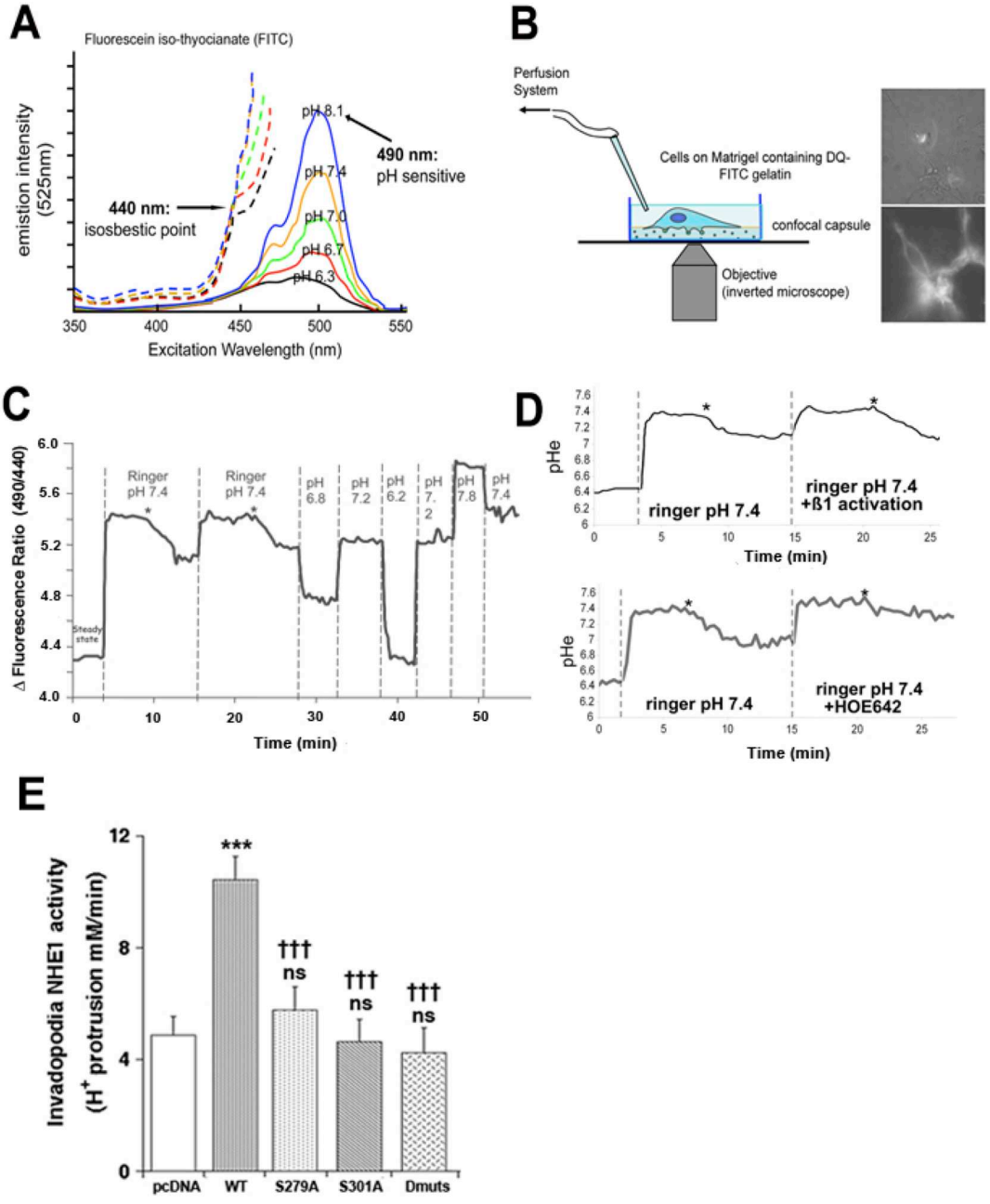

Fig. 2. S279 and S301 of NHERF1 account for NHE1-dependent extracellular acidification at the invadopodia.
The pH of areas of extracellular proteolysis was measured by fluorescence ratio imaging of unquenched fluorescein-conjugated gelatin DQ(FITC)-gelatin, that had been liberated by proteolysis of the ECM in which it was dissolved. In brief, Matrigel™ (ice cold) was diluted to 4 mg/ml with ice-cold serum free DMEM and DQ-FITC-gelatin (final concentration of 30 μg/ml). (A) Images were acquired with 490 nm (pH-sensitive) and 440 nm (isosbestic pH-insensitive) excitation wavelength filters, using a 535 nm emission filter. The use of the ratio of pH-sensitive and pH-insensitive signals permits an analysis of pH that is continuously corrected for any changes in probe concentration that could occur during the experiment. (B) Scheme of the experimental apparatus. (C) Digested areas were selected and after signal stabilization (to determine the steady state ratio value), an extracellular alkalinization (dashed line) was produced by perfusing the cell layer with a NaCl Ringer solution (in mM: 140 NaCl, 5 KCl, 20 HEPES, 10 D-Glucose, 0.1 $CaCl_2$, and 1 $MgCl_2$) at pH 7.4 in which the fluid level of the dish was maintained by needle aspiration and extracellular pH (pHe) was followed over time. When the values were stable, perfusion was halted (asterisk) and the ability of the cells to acidify the ECM was measured and the process repeated to determine the reproducibility. After each experiment, *in situ* calibration curves were obtained by perfusing the cells with ringer solutions having different pH (6.2; 6.8; 7.2; 7.4; 7.8). The background ratio was subtracted from each ratio value in each analyzed area, and the calibration ratio values were used to build a calibration curve to convert each ratio value into a pH value. (D) extracellular matrix acidification occurred a few minutes after stopping perfusion with ringer pH 7.4 and this acidification was stimulated by β1-integrin activation with the P4G11 antibody (5 μg/ml, upper panel) and reduced by the NHE1 specific inhibitor HOE642 (500 nM, lower panel). (E) NHE1 activity was measured as proton (H^+) extrusion into the ECM measured with a technique based on the pH sensitivity of released FITC from quenched DQ(FITC)-gelatin dissolved in the Matrigel™. Data are mean ± SEM, n = 7.

closed areas (lacunae, asterisk). This ability was abrogated in WT-NHERF1 and the over-expressing cells. The S279A mutant generated short, thin cord-like structures issuing out of the nodes, but did not form any lacunae while the S301A mutant initiated the formation of capillary-like networks but these had few nodes and few lacunae. In contrast, the VM ability was completely restored in the Dmuts cells, similarly to that previously reported in HRF2 cells [30]. These data demonstrate that the double phosphorylation of S279 and S301 of

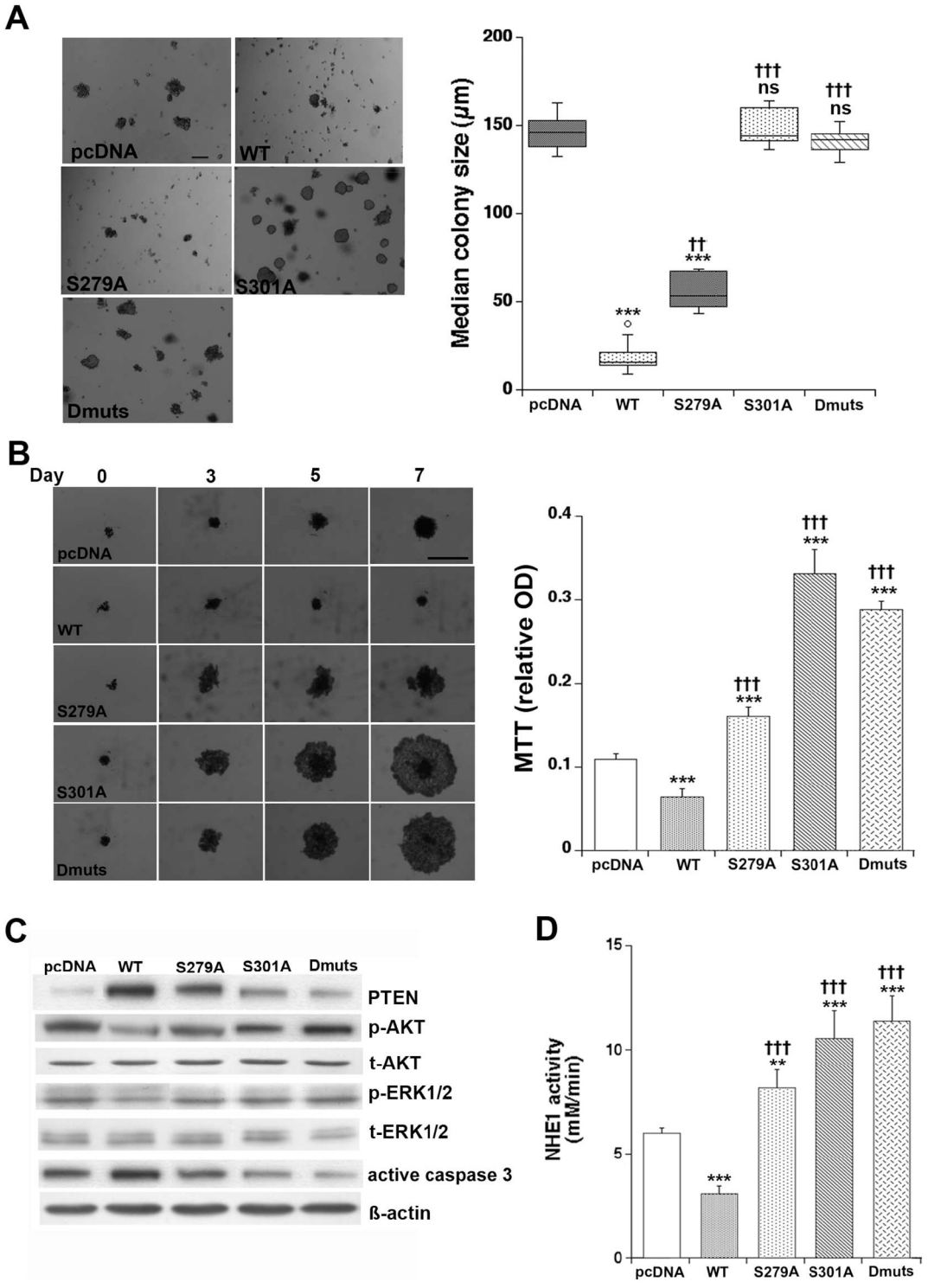

Fig. 3. S279 and S301 of NHERF1 oppositely regulate anchorage-independent colony and 3D spheroid growth.
The indicated MDA-MB-231 clones stably expressing the empty vector (pcDNA), WT-NHERF1 (WT), the S279A- and the S301A-mutated constructs and the double S279A/S301A mutated construct (Dmuts) were either plated onto soft-agar (A) or seeded into round bottom extra low adhesion 96 well plates (B).
(A) After 3 weeks, colony number counts and size were measured using Image J software. Left panel: representative photomicrographs of colonies for each cell variant (bar, 10 μm). Right panel: the box plots indicating the median, first and third quartile of colony size and whiskers indicate minimum and maximum values, n = 4; ***$p < 0.001$ compared to pcDNA and $^{††}p < 0.01$, $^{†††}p < 0.001$ compared to the WT. (B) Left panel: representative photomicrographs of spheroids for each cell variant at 0, 3, 5 and 7 days growth (bar, 10 μm). Right panel: spheroid growth of the different clones measured as MTT incorporation. Data are mean ± SEM, n = 4; ***$p < 0.001$ compared to pcDNA and $^{††}p < 0.01$, $^{†††}p < 0.001$ compared to the WT clone. (C) Representive Western Blots for PTEN, phospho and total AKT and phospho and total ERK1/2, active Caspase 3 and β-Actin. (D) NHE1 activity was measured as changes in pHi after the addition of 130 mM NaCl in NH_4Cl-acidified clones in a Hank's solution in absence of NaCl measured using the pH-sensitive cell permeant BCECF-AM probe. Data are mean ± SEM of H^+ efflux, n = 6, **$p < 0.01$, ***$p < 0.001$ compared to pcDNA and $^{†††}p < 0.001$ compared to the WT clone.

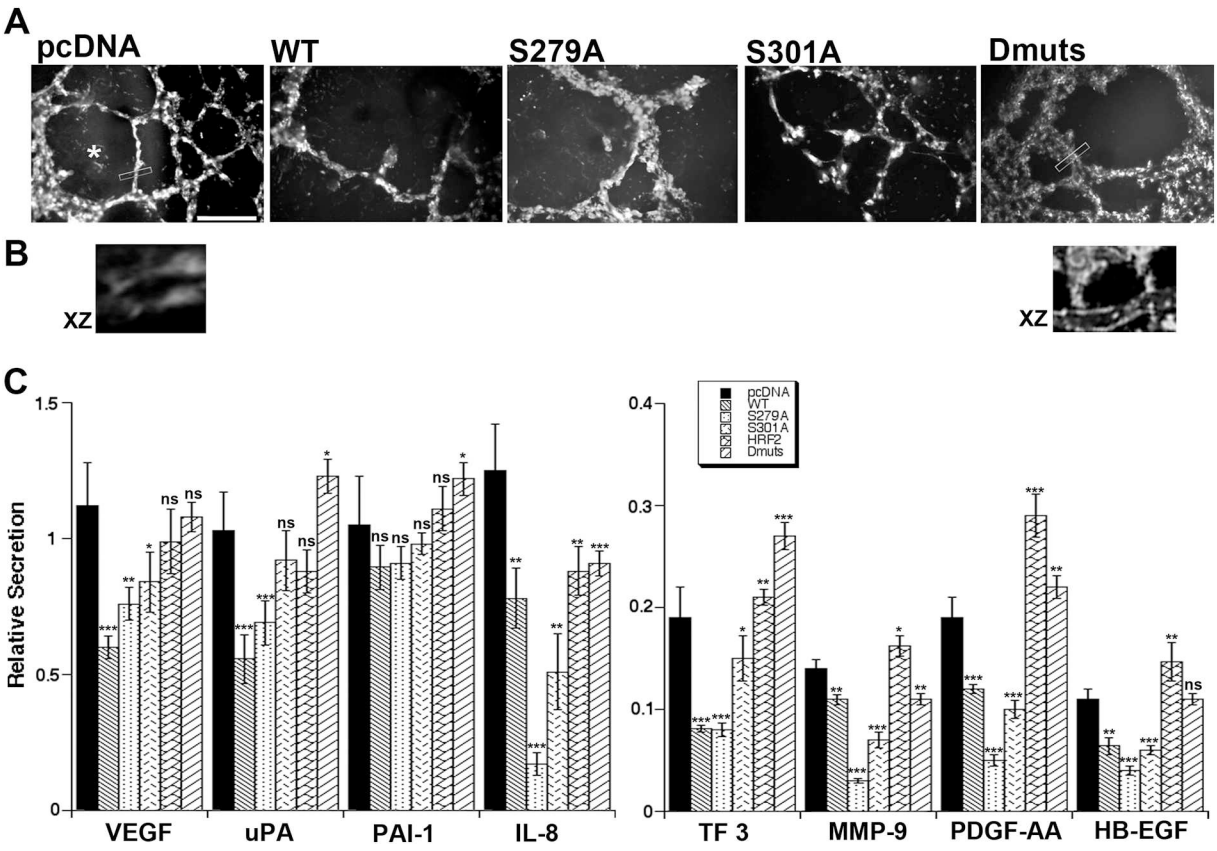

Fig. 4. NHERF1 inhibits vasculogenic mimicry-like ability principally through the phosphorylable S301.
(A) Representative microphotographs of capillary-like tubule formations obtained when cells were seeded inside Matrigel™ for 5 days. Cell membranes were stained with Oregon Green® 488 DHPE and acquired by confocal microscopy. Asterisks indicate empty areas (lacunae) bordered by the capillary-like network. Bar, 10 μm. (B) Panels are XZ-zoomed vertical cross-section views of 3D reconstruction of z-stacked VM tubes of the regions of interest indicated by the open rectangle in the field from pcDNA cells and Dmuts cells. Vertical sections of the 3D-reconstructed tubes show that they are open lumen-like structures surrounded by fluorescent cells. (C) Substitution of phosphorylable S279 and S301 to alanine residues altered angiogenic secretion pattern in conditioned media. Results are expressed as mean ± SEM, n = 4, *p < 0.05, **p < 0.01, ***p < 0.001 compared to pcDNA.

NHERF1 is necessary for the development of the VM network.

As both angiogenesis and VM can be regulated by the autocrine release of angiogenic factors [60–62], we next analyzed both pro- and anti-angiogenic factor levels in conditioned media of the different clones (Fig. 4C). In line with the pattern of VM, the pcDNA clone cells had a high release of pro-angiogenic factors (VEGF, uPA, TF3, IL-8, HB-EGF and PDGF-AA), which were significantly reduced (from 30% to 80% decrease) in the WT and S279A clones. The increasing VM observed from the S279A to the S301A mutants and finally to the Dmuts was associated with a step-wise increase in the secretion of all factors, such that the Dmuts cells had levels and a release pattern very similar to the pcDNA cells. Importantly, both the released factors and their levels of secretion of the Dmuts clone were very similar to that found in the HRF2 clone.

3.4. Phosphorylable S279 and S301 of NHERF1 orchestrates in vivo metastasis dynamics and organotropism

We then tested whether the S279 and S301 of NHERF1 could determine the ability of cancer cells to develop experimental metastases *in vivo*. For this, control pcDNA, WT-NHERF1 or Dmuts cells, all expressing the luciferase gene at comparable levels (data not shown), were injected in the tail vein of NMRI SCID Beige nude mice. The colonization of mouse organs was followed *in vivo* by bioluminescent imaging (BLI), after luciferin injection, every week for a total duration of 8 weeks (Fig. 5A). BLI analyses from living animals indicated that pcDNA cancer cells formed fewer metastases (4/8 mice), in the chest area, compared with WT-NHERF1 cells which rapidly invaded and strongly colonized this region (8/8 mice). In contrast, Dmuts cells, which demonstrated inhibited invasion and invadopodia function (Figs. 1 and 2), but increased vasculogenic mimicry (Fig. 4), showed metastases in 6/8 mice but with a significantly reduced signal (Fig. 5A). At completion of the study, isolated organs (lungs, brain, liver, bones from rachis/ribs and legs) were analyzed *ex vivo* by BLI (Fig. 5B). Control (pcDNA) cells demonstrated a predominant lung colonization and very low bone colonization. WT-NHERF1 cells showed an increased total metastatic behavior, but with a similar organotropism to pcDNA cells. In comparison, Dmuts cells had a strongly reduced total metastatic potency (Fig. 5A) and were redirected towards bone colonization compared to both pcDNA and WT-NHERF1 cells (Fig. 5B). Immunohistochemical analyses of human cytokeratin 7 staining in lungs (Fig. 5C), indicated that the strong lung metastatic load observed in mice injected with WT-NHERF1 cells (Fig. 5D, left panel), was due to a large number (Fig. 5D, middle panel) of small metastases (Fig. 4D, right panel), which verified results obtained in soft-agar and 3D spheroids (Fig. 3). Importantly, Dmuts cells formed lung metastases with similar size than those induced by pcDNA cells (Fig. 5D, right panel), but a low number of foci (Fig. 5D, middle panel). These results indicate that phosphorylable S279 and S301 of NHERF1 control both metastatic potency and organotropism.

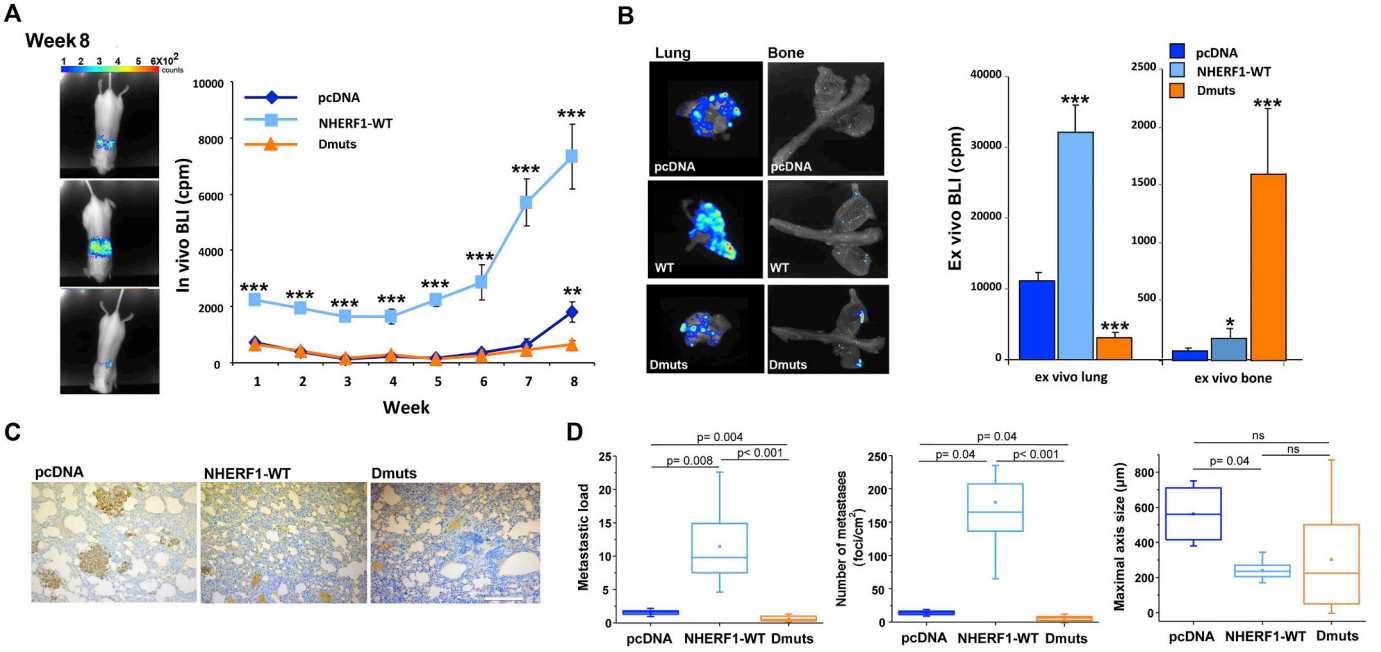

Fig. 5. NHERF1 phosphorylation dictates levels and organotropism pattern of metastasis.
Six-week-old female NMRI mice were inoculated in the lateral tail vein with a suspension of pcDNA, WT, and Dmuts clone cells. n = 8 mice/group. (A) Left panel: Representative *in vivo* BLI 8th week after cell injection in living animals. Right panel: Mean *in vivo* BLI value (expressed in cpm) as a function of time, recorded in the whole body of mice coming from the three groups, mean ± SEM, n = 8, **p < 0.01, ***p < 0.001 compared to pcDNA (B) Left panel: representative *ex vivo* BLI after lung and rachis/rib dissection isolation, at completion of the study (8th week). Right Panel: BLI quantification of excised lungs. Mean ± SEM, n = 8, *p < 0.05, ***p < 0.001 compared to pcDNA of each organ. (C) Representative staining of tumor sections from lung metastases with anti-human cytokeratin 7 (brown staining) to identify human breast cancer cells and counterstained with haematoxylin (blue labelling). Scale bar, 100 µm. (D) Analyses of metastatic load, number and size of metastases in lungs for the MDA-MB-231 NHERF1 clones. Values are the mean ± S.E.M. of four animals for pcDNA and 8 animals for WT-NHERF1 and double mutants (Dmuts).

4. Discussion

The complex set of processes required to produce metastatic lesions is based on tumor cell phenotypic plasticity, which enables the cell to acquire pro-metastatic phenotypes and organotropism [3,63,64]. This plasticity relies on specific signal transduction systems [65] which are orchestrated by scaffolding proteins. NHERF1 has been shown to finely regulate the various metastatic behaviors of cancer cells [6,7,30] and this capacity was demonstrated to occur through its PDZ binding domains, permitting the shift from one to another phenotypic outcome, and thus conferring a specific metastatic competence to the cell [24,30]. However, the *in situ* mechanism(s) underlying this regulation of PDZ function is still only partially known [32,66].

Here, we have identified the phosphorylable S279 and S301 of NHERF1 as key determinants in the regulation of metastatic phenotype expression and organotropic outcome. S279A and S301A phosphorylation-dead NHERF1 mutant-expressing cancer cells have (*i*) a greatly reduced invasive capacity (Figs. 1 and 2), suggesting that the cooperative action of phosphorylation at S279 and S301 of NHERF1 are necessary for these properties; (*ii*) a release of the inhibition of anchorage-independent tumor growth observed in WT NHERF1-overexpressing cells, especially by the phosphorylation of S301 (Fig. 3); (*iii*) an increased ability to form tumor vascular channel-like structures (Fig. 4A–B); together with (*iv*) changes in angiogenic factor secretion (Fig. 4C), and finally (*v*) a switch in metastatic organotropic choice. Indeed, cells over-expressing WT-NHERF1 displayed a greatly enhanced lung metastatic load consisting of high numbers of micro-metastases, while cells over-expressing the NHERF1 double S279A/S301A mutant were almost completely redirected towards bone metastasis (*i.e.* high osteotropism) (Fig. 5).

The phosphorylation of NHERF1 serines 279 and 301 has been shown to be mediated by the cdc2/cyclin B kinase [31–33] and is involved in NHERF1 ability to oligomerize during mitosis [31], in NHERF1 increased proteosomal degradation (by human papillomavirus oncoproteins) and subsequent PI3K/AKT signaling pathway activation [33] and in actin cytoskeleton remodelling and cell-ECM adherence [32]. We indeed found that cdc2/cyclin B kinase is involved in phosphoNHERF1-driven regulation of both anchorage-independent 3D growth and invadopodia-mediated ECM digestion since incubation of WT-NHERF1 cells with the cdc2 kinase inhibitor, roscovitine, dose-dependently decreases NHERF1 phosphorylation and replicates the increase in anchorage-independent growth and decrease in invadopodia proteolytic activity observed in the Dmut clone (Supplemental Fig. 3).

Human breast cancer cells are able to form vasculogenic mimicry (VM)-like channels, and overexpression of WT-NHERF1 impairs this ability through its PDZ2 binding domain (HRF2 clone) [30]. Importantly, VM and angiogenic secretome are increasingly regulated by S279 and S301, such that the double S279A/S301A mutant, like the PDZ2 mutant, fully restored these abilities. These results suggest that NHERF1 can orchestrate, *via* reversible phosphorylation, a bidirectional transition program called “mesenchymal-vasculogenic transition” [30,67,68]. This transition could, in part, be regulated by the release of pro-angiogenic molecules. Since VM was reported to be resistant to angiogenesis inhibitors in tumor therapy [68,69], elucidation of molecular mechanisms by which deregulated NHERF1 signaling promotes both angiogenesis and VM could open new therapeutic strategies against tumor microcirculation.

In mice injected with WT-NHERF1 cells, the high lung metastatic load was due to a high number of micro-metastases, and not to the

growth of large metastatic foci. On the contrary, mice injected with Dmuts cells, showed a lower number of lung metastases, but with a size similar to the pcDNA-injected mice (Fig. 5). These data, together with those of the 3D growth (Fig. 3) and VM (Fig. 4), suggest that WT-NHERF1 activates an invasive program allowing cells to infiltrate extracellular matrices, but restrains growth signals. These results further validate the participation of the "mesenchymal-endothelial transition" as a critical step in determining metastatic bone tropism. The vasculogenic program might confer an additional advantage in the highly hypoxic microenvironments, such as in bone [70–75]. The secondary organ selection might arise depending on a combination of (*i*) the increased ability to enter the secondary tissue *via* invasion; (*ii*) the growth when in place (3D anchorage-independent growth), especially in lungs, and (*iii*) the angiogenic competence (VM, angiogenic secretome), especially in bones. In this scenario, an increased invasion would facilitate lung metastases, but with limited outgrowth capacity due to increased apoptosis [30] and reduced angiogenesis, while the increased VM/proangiogenic secretome together with increased 3D growth would facilitate bone metastases. Importantly, our data support the idea that plasticity in growth/invasion/metastasis cannot be explained solely by a "minority" population driving the events, but that epigenetic alterations can define tumor cell "phenotype" and are important for the "selection of the preferred" [76].

In conclusion, we report here that NHERF1 plays an important role in malignant progression *via* phosphorylable serine residues 279 and 301. We hypothesize that metastatic cells respond to the different microenvironments of secondary organs through the modulation of NHERF1 phosphorylation, thus altering their phenotypic outcome [30]. The understanding of the specific environmental conditions and the mechanisms driving these phosphorylations in different tumors will be an important line of future research. These findings also suggest that NHERF1 phosphorylation state may constitute a target for the development of new therapies in order to prevent and/or reduce the metastatic spreading of cancer cells.

Supplementary data to this article can be found online at https://doi.org/10.1016/j.bbadis.2018.10.017.

Conflicts of interest

Authors declare no conflict of interest.

Author contributions

SJR, RAC and SR conceived the project, designed experiments and supervised research. MRG, EB and RR performed most of the experiments and analyzed data. MB-G and M-LC performed the *in vivo* Zebrafish experiments and SM-L, TO, GF and RG the *in vivo* mouse experiments. MRG, SC and LC contributed to invadopodia, invasion, soft agar/spheroid and WB experiments. SJR, RAC and SR wrote the manuscript.

Transparency document

The Transparency document associated with this article can be found, in online version.

Acknowledgements

This work was supported by "Associazione Italiana per la Ricerca sul Cancro" grant #11348 to SJR and by the Inserm, the Région Centre-Val de Loire, the "Ligue Nationale contre le Cancer", the "Association CANCEN", and the "Prix Ruban Rose Avenir 2017" to SR. The SJR laboratory is part of the Italian network "Istituto Nazionale Biostrutture e Biosistemi" (INBB), the Centro di Eccellenza di Genomica in Campo Biomedico ed Agrario of the University of Bari and the project BioBoP of the Region Puglia. Action Co-founded by Cohesion and Development Fund 2007–2013 – APQ Research Puglia Region "Regional programme supporting smart specialization and social and environmental sustainability – Future In Research". SJR obtained a professor fellowship at the University of Tours.

UNIONE EUROPEA

REGIONE PUGLIA

SMARTPUGLIA INTELLIGENTI DAL FUTURO

·a·r·t·i· Agenzia regionale per la tecnologia e l'innovazione

Unlabelled Image

References

[1] T.R. Geiger, D.S. Peeper, Metastasis mechanisms, Biochim. Biophys. Acta 1796 (2009) 293–308.
[2] A.C. Obenauf, J. Massague, Surviving at a distance: organ specific metastasis, Trends Cancer 1 (2015) 76–91.
[3] J. Massague, A.C. Obenauf, Metastatic colonization by circulating tumour cells, Nature 529 (2016) 298–306.
[4] E. Bon, V. Driffort, F. Gradek, C. Martinez-Caceres, M. Anchelin, P. Pelegrin, M.L. Cayuela, S. Marionneau-Lambot, T. Oullier, R. Guibon, G. Fromont, J.L. Gutierrez-Pajares, I. Domingo, E. Piver, A. Moreau, J. Burlaud-Gaillard, P.G. Frank, S. Chevalier, P. Besson, S. Roger, SCN4B acts as a metastasis-suppressor gene preventing hyperactivation of cell migration in breast cancer, Nat. Commun. 7 (2016) 13648.
[5] J. Jin, X. Xie, C. Chen, J.G. Park, C. Stark, D.A. James, M. Olhovsky, R. Linding, Y. Mao, T. Pawson, Eukaryotic protein domains as functional units of cellular evolution, Sci. Signal. 2 (2009) ra76.
[6] Y. Ivarsson, Plasticity of PDZ domains in ligand recognition and signaling, FEBS Lett. 586 (2012) 2638–2647.
[7] V. Astro, I. de Curtis, Plasma membrane-associated platforms: dynamic scaffolds that organize membrane-associated events, Sci. Signal. 8 (2015) re1.
[8] R.A. Cardone, A. Bellizzi, G. Busco, E.J. Weinman, M.E. Dell'Aquila, V. Casavola, A. Azzariti, A. Mangia, A. Paradiso, S.J. Reshkin, The NHERF1 PDZ2 domain regulates PKA-RhoA-p38-mediated NHE1 activation and invasion in breast tumor cells, Mol. Biol. Cell 18 (2007) 1768–1780.
[9] J. Song, J. Bai, W. Yang, E.W. Gabrielson, D.W. Chan, Z. Zhang, Expression and clinicopathological significance of oestrogen-responsive ezrin-radixin-moesin-binding phosphoprotein 50 in breast cancer, Histopathology 51 (2007) 40–53.
[10] T. Karn, E. Ruckhaberle, L. Hanker, V. Muller, M. Schmidt, C. Solbach, R. Gatje, M. Gehrmann, U. Holtrich, M. Kaufmann, A. Rody, Gene expression profiling of luminal B breast cancers reveals NHERF1 as a new marker of endocrine resistance, Breast Cancer Res. Treat. 130 (2011) 409–420.
[11] A.D. Tabrizi, S.E. Kalloger, M. Kobel, J. Cipollone, C.D. Roskelley, E. Mehl, C.B. Gilks, Primary ovarian mucinous carcinoma of intestinal type: significance of pattern of invasion and immunohistochemical expression profile in a series of 31 cases, Int. J. Gynecol. Pathol. 29 (2010) 99–107.
[12] A. Bellizzi, M.R. Greco, R. Rubino, A. Paradiso, S. Forciniti, K. Zeeberg, R.A. Cardone, S.J. Reshkin, The scaffolding protein NHERF1 sensitizes EGFR-dependent tumor growth, motility and invadopodia function to gefitinib treatment in breast cancer cells, Int. J. Oncol. 46 (2015) 1214–1224.
[13] M.M. Georgescu, F.C. Morales, J.R. Molina, Y. Hayashi, Roles of NHERF1/EBP50 in cancer, Curr. Mol. Med. 8 (2008) 459–468.

[14] A. Paradiso, E. Scarpi, A. Malfettone, T. Addati, F. Giotta, G. Simone, D. Amadori, A. Mangia, Nuclear NHERF1 expression as a prognostic marker in breast cancer, Cell Death Dis. 4 (2013) e904.
[15] C. Saponaro, A. Malfettone, T.S. Dell'Endice, A.E. Brunetti, P. Achimas-Cadariu, A. Paradiso, A. Mangia, The prognostic value of the Na(+)/H(+) exchanger regulatory factor 1 (NHERF1) protein in cancer, Cancer Biomark. 14 (2014) 177–184.
[16] M. Ji, D. Fan, L. Yuan, Y. Zhang, W. Dong, X. Peng, EBP50 inhibits pancreatic cancer cell growth and invasion by targeting the beta-catenin/E-cadherin pathway, Exp. Ther. Med. 10 (2015) 1311–1316.
[17] Q. Ma, Y. Jiao, Y. Hao, S. Yan, N. Lyu, H. Gao, D. Li, Q. Liu, J. Zheng, N. Song, Targeting of through RNA interference inhibits the proliferation and migration of metastatic prostate cancer cells, Oncol. Lett. 11 (2016) 1149–1154.
[18] J. Vaquero, T.H. Nguyen Ho-Bouldoires, A. Claperon, L. Fouassier, Role of the PDZ-scaffold protein NHERF1/EBP50 in cancer biology: from signaling regulation to clinical relevance, Oncogene 36 (2017) 3067–3079.
[19] A. Mangia, E. Scarpi, G. Partipilo, L. Schirosi, G. Opinto, F. Giotta, G. Simone, NHERF1 together with PARP1 and BRCA1 expression as a new potential biomarker to stratify breast cancer patients, Oncotarget 8 (2017) 65730–65742.
[20] S. Shenolikar, J.W. Voltz, R. Cunningham, E.J. Weinman, Regulation of ion transport by the NHERF family of PDZ proteins, Physiology (Bethesda) 19 (2004) 362–369.
[21] Y. Pan, L. Wang, J.L. Dai, Suppression of breast cancer cell growth by Na^+/H^+ exchanger regulatory factor 1 (NHERF1), Breast Cancer Res. 8 (2006) R63.
[22] H.C. Lim, T.S. Jou, Ras-activated RSK1 phosphorylates EBP50 to regulate its nuclear localization and promote cell proliferation, Oncotarget 7 (2016) 10283–10296.
[23] R.A. Cardone, M.R. Greco, K. Zeeberg, A. Zaccagnino, M. Saccomano, A. Bellizzi, P. Bruns, M. Menga, P. Pilarsky, A. Schwab, F. Alves, H. Kalthoff, V. Casavola, S.J. Reshkin, A novel NHE1-centered signaling cassette drives epidermal growth factor receptor–dependent pancreatic tumor metastasis and is a target for combination therapy, Neoplasia 17 (2015) 155–166.
[24] G. Du, Y. Gu, C. Hao, Z. Yuan, J. He, W.G. Jiang, S. Cheng, The cellular distribution of Na^+/H^+ exchanger regulatory factor 1 is determined by the PDZ-I domain and regulates the malignant progression of breast cancer, Oncotarget 7 (2016) 29440–29453.
[25] J.R. Molina, F.C. Morales, Y. Hayashi, K.D. Aldape, M.M. Georgescu, Loss of PTEN binding adapter protein NHERF1 from plasma membrane in glioblastoma contributes to PTEN inactivation, Cancer Res. 70 (2010) 6697–6703.
[26] J.F. Zheng, L.C. Sun, H. Liu, Y. Huang, Y. Li, J. He, EBP50 exerts tumor suppressor activity by promoting cell apoptosis and retarding extracellular signal-regulated kinase activity, Amino Acids 38 (2010) 1261–1268.
[27] K.L. Kislin, W.S. McDonough, J.M. Eschbacher, B.A. Armstrong, M.E. Berens, NHERF-1: modulator of glioblastoma cell migration and invasion, Neoplasia 11 (2009) 377–387.
[28] N. Asp, A. Kvalvaag, K. Sandvig, S. Pust, Regulation of ErbB2 localization and function in breast cancer cells by ERM proteins, Oncotarget 7 (2016) 25443–25460.
[29] G. Du, C. Hao, Y. Gu, Z. Wang, W.G. Jiang, J. He, S. Cheng, A. Novel, NHERF1 mutation in human breast cancer inactivates inhibition by NHERF1 protein in EGFR signaling, Anticancer Res. 36 (2016) 1165–1173.
[30] R.A. Cardone, M.R. Greco, M. Capulli, E.J. Weinman, G. Busco, A. Bellizzi, V. Casavola, E. Antelmi, B. Ambruosi, M.E. Dell'Aquila, A. Paradiso, A. Teti, N. Rucci, S.J. Reshkin, NHERF1 acts as a molecular switch to program metastatic behavior and organotropism via its PDZ domains, Mol. Biol. Cell 23 (2012) 2028–2040.
[31] J. He, A.G. Lau, M.B. Yaffe, R.A. Hall, Phosphorylation and cell cycle-dependent regulation of Na^+/H^+ exchanger regulatory factor-1 by Cdc2 kinase, J. Biol. Chem. 276 (2001) 41559–41565.
[32] C. Sun, J. Zheng, S. Cheng, D. Feng, J. He, EBP50 phosphorylation by Cdc2/Cyclin B kinase affects actin cytoskeleton reorganization and regulates functions of human breast cancer cell line MDA-MB-231, Mol. Cell 36 (2013) 47–54.
[33] R. Accardi, R. Rubino, M. Scalise, T. Gheit, N. Shahzad, M. Thomas, L. Banks, C. Indiveri, B.S. Sylla, R.A. Cardone, S.J. Reshkin, M. Tommasino, E6 and E7 from human papillomavirus type 16 cooperate to target the PDZ protein Na/H exchange regulatory factor 1, J. Virol. 85 (2011) 8208–8216.
[34] E.J. Weinman, Y. Wang, F. Wang, C. Greer, D. Steplock, S. Shenolikar, A C-terminal PDZ motif in NHE3 binds NHERF-1 and enhances cAMP inhibition of sodium-hydrogen exchange, Biochemistry 42 (2003) 12662–12668.
[35] L. Brisson, L. Gillet, S. Calaghan, P. Besson, J.Y. Le Guennec, S. Roger, J. Gore, Na(V)1.5 enhances breast cancer cell invasiveness by increasing NHE1-dependent H(+) efflux in caveolae, Oncogene 30 (2011) 2070–2076.
[36] V. Driffort, L. Gillet, E. Bon, S. Marionneau-Lambot, T. Oullier, V. Joulin, C. Collin, J.C. Pages, M.L. Jourdan, S. Chevalier, P. Bougnoux, J.Y. Le Guennec, P. Besson, S. Roger, Ranolazine inhibits NaV1.5-mediated breast cancer cell invasiveness and lung colonization, Mol. Cancer 13 (2014) 264.
[37] G. Busco, R.A. Cardone, M.R. Greco, A. Bellizzi, M. Colella, E. Antelmi, M.T. Mancini, M.E. Dell'Aquila, V. Casavola, A. Paradiso, S.J. Reshkin, NHE1 promotes invadopodial ECM proteolysis through acidification of the peri-invadopodial space, FASEB J. 24 (2010) 3903–3915.
[38] P. Montcourrier, P.H. Mangeat, C. Valembois, G. Salazar, A. Sahuquet, C. Duperray, H. Rochefort, Characterization of very acidic phagosomes in breast cancer cells and their association with invasion, J. Cell Sci. 107 (Pt 9) (1994) 2381–2391.
[39] B. Jelassi, A. Chantome, F. Alcaraz-Perez, A. Baroja-Mazo, M.L. Cayuela, P. Pelegrin, A. Surprenant, S. Roger, P2X(7) receptor activation enhances SK3 channels- and cystein cathepsin-dependent cancer cells invasiveness, Oncogene 30 (2011) 2108–2122.
[40] H. Hamidi, J. Ivaska, Vascular morphogenesis: an integrin and fibronectin highway, Curr. Biol. 27 (2016) R158–R161.
[41] D. Bianconi, M. Unseld, G.W. Prager, Integrins in the spotlight of Cancer, Int. J. Mol. Sci. 17 (2016).
[42] E. Antelmi, R.A. Cardone, M.R. Greco, R. Rubino, F. Di Sole, N.A. Martino, V. Casavola, M. Carcangiu, L. Moro, S.J. Reshkin, ss1 integrin binding phosphorylates ezrin at T567 to activate a lipid raft signalsome driving invadopodia activity and invasion, PLoS One 8 (2013) e75113.
[43] L. Sevenich, J.A. Joyce, Pericellular proteolysis in cancer, Genes Dev. 28 (2015) 2331–2347.
[44] L. Brisson, S.J. Reshkin, J. Gore, S. Roger, pH regulators in invadosomal functioning: proton delivery for matrix tasting, Eur. J. Cell Biol. 91 (2012) 847–860.
[45] D. Hoshino, K.M. Branch, A.M. Weaver, Signaling inputs to invadopodia and podosomes, J. Cell Sci. 126 (2013) 2979–2989.
[46] B.T. Beaty, J. Condeelis, Digging a little deeper: the stages of invadopodium formation and maturation, Eur. J. Cell Biol. 93 (2014) 438–444.
[47] L. Brisson, V. Driffort, L. Benoist, M. Poet, L. Counillon, E. Antelmi, R. Rubino, P. Besson, F. Labbal, S. Chevalier, S.J. Reshkin, J. Gore, S. Roger, NaV1.5 Na(+) channels allosterically regulate the NHE-1 exchanger and promote the activity of breast cancer cell invadopodia, J. Cell Sci. 126 (2013) 4835–4842.
[48] F. Lucien, K. Brochu-Gaudreau, D. Arsenault, K. Harper, C.M. Dubois, Hypoxia-induced invadopodia formation involves activation of NHE-1 by the p90 ribosomal S6 kinase (p90RSK), PLoS One 6 (2011) e28851.
[49] C.C. Mader, M. Oser, M.A. Magalhaes, J.J. Bravo-Cordero, J. Condeelis, A.J. Koleske, H. Gil-Henn, An EGFR-Src-Arg-Cortactin pathway mediates functional maturation of invadopodia and breast cancer cell invasion, Cancer Res. 71 (2011) 1730–1741.
[50] M. Sharma, A. Dube, H. Bansal, P. Kumar Gupta, Effect of pH on uptake and photodynamic action of chlorin p6 on human colon and breast adenocarcinoma cell lines, Photochem. Photobiol. Sci. 3 (2004) 231–235.
[51] H.H. Fiebig, A. Maier, A.M. Burger, Clonogenic assay with established human tumour xenografts: correlation of in vitro to in vivo activity as a basis for anticancer drug discovery, Eur. J. Cancer 40 (2004) 802–820.
[52] J.R. Molina, N.K. Agarwal, F.C. Morales, Y. Hayashi, K.D. Aldape, G. Cote, M.M. Georgescu, PTEN, NHERF1 and PHLPP form a tumor suppressor network that is disabled in glioblastoma, Oncogene 31 (2012) 1264–1274.
[53] W. Yao, D. Feng, W. Bian, L. Yang, Y. Li, Z. Yang, Y. Xiong, J. Zheng, R. Zhai, J. He, EBP50 inhibits EGF-induced breast cancer cell proliferation by blocking EGFR phosphorylation, Amino Acids 43 (2012) 2027–2035.
[54] J. Zheng, Y. Dai, Z. Yang, L. Yang, Z. Peng, R. Meng, Y. Xiong, J. He, Ezrin-radixin-moesin-binding phosphoprotein-50 regulates EGF-induced AKT activation through interaction with EGFR and PTEN, Oncol. Rep. 35 (2016) 530–537.
[55] Y. Wang, Z. Peng, R. Meng, T. Tao, Q. Wang, C. Zhao, H. Liu, R. Song, J. Zheng, Q. Qin, J. He, NHERF1 inhibits proliferation of triple-negative breast cancer cells by suppressing GPER signaling, Oncol. Rep. 38 (2017) 221–228.
[56] M. Flinck, S.H. Kramer, S.F. Pedersen, Roles of pH in control of cell proliferation, Acta Physiol (Oxford) 223 (2018) e13068.
[57] M. Flinck, S.H. Kramer, J. Schnipper, A.P. Andersen, S.F. Pedersen, The acid-base transport proteins NHE1 and NBCn1 regulate cell cycle progression in human breast cancer cells, Cell Cycle 17 (2018) 1056–1067.
[58] S.D. Harguindey S, J. Devesa, K. Alfarouk, R.A. Cardone, J.D. Polo Orozco, P. Devesa, C. Rauch, G. Orive, E. Anitua, S. Roger, S.J. Reshkin, Cellular acidification as a new approach to cancer treatment and to the understanding and therapeutics of neurodegenerative diseases, Semin. Cancer Biol. 11 (2017) (pii: S1044-579X(17)30019-6).
[59] Y. Shen, J. Quan, M. Wang, S. Li, J. Yang, M. Lv, Z. Chen, L. Zhang, X. Zhao, Tumor vasculogenic mimicry formation as an unfavorable prognostic indicator in patients with breast cancer, Oncotarget 8 (2017) 56408–56416.
[60] T.B. Schaaij-Visser, M. de Wit, S.W. Lam, C.R. Jimenez, The cancer secretome, current status and opportunities in the lung, breast and colorectal cancer context, Biochim. Biophys. Acta 1834 (2013) 2242–2258.
[61] M.B. Patel, S.P. Pothula, Z. Xu, A.K. Lee, D. Goldstein, R.C. Pirola, M.V. Apte, J.S. Wilson, The role of the hepatocyte growth factor/c-MET pathway in pancreatic stellate cell-endothelial cell interactions: antiangiogenic implications in pancreatic cancer, Carcinogenesis 35 (2014) 1891–1900.
[62] C. Barcena, M. Stefanovic, A. Tutusaus, G.A. Martinez-Nieto, L. Martinez, C. Garcia-Ruiz, A. de Mingo, J. Caballeria, J.C. Fernandez-Checa, M. Mari, A. Morales, Angiogenin secretion from hepatoma cells activates hepatic stellate cells to amplify a self-sustained cycle promoting liver cancer, Sci. Rep. 5 (2015) 7916.
[63] A.J. Minn, G.P. Gupta, D. Padua, P. Bos, D.X. Nguyen, D. Nuyten, B. Kreike, Y. Zhang, Y. Wang, H. Ishwaran, J.A. Foekens, M. van de Vijver, J. Massague, Lung metastasis genes couple breast tumor size and metastatic spread, Proc. Natl. Acad. Sci. U. S. A. 104 (2007) 6740–6745.
[64] Y. Kang, P.M. Siegel, W. Shu, M. Drobnjak, S.M. Kakonen, C. Cordon-Cardo, T.A. Guise, J. Massague, A multigenic program mediating breast cancer metastasis to bone, Cancer Cell 3 (2003) 537–549.
[65] A.J. Firestone, J.K. Chen, Controlling destiny through chemistry: small-molecule regulators of cell fate, ACS Chem. Biol. 5 (2010) 15–34.
[66] G.J. Song, K.L. Leslie, S. Barrick, T. Mamonova, J.M. Fitzpatrick, K.W. Drombosky, N. Peyser, B. Wang, M. Pellegrini, P.M. Bauer, P.A. Friedman, D.F. Mierke, A. Bisello, Phosphorylation of ezrin-radixin-moesin-binding phosphoprotein 50 (EBP50) by Akt promotes stability and mitogenic function of S-phase kinase-

associated protein-2 (Skp2), J. Biol. Chem. 290 (2015) 2879–2887.
[67] L. Sun, J. Zheng, Q. Wang, R. Song, H. Liu, R. Meng, T. Tao, Y. Si, W. Jiang, J. He, NHERF1 regulates actin cytoskeleton organization through modulation of alpha-actinin-4 stability, FASEB J. 30 (2016) 578–589.
[68] M.J. Hendrix, E.A. Seftor, R.E. Seftor, J.T. Chao, D.S. Chien, Y.W. Chu, Tumor cell vascular mimicry: novel targeting opportunity in melanoma, Pharmacol. Ther. 159 (2016) 83–92.
[69] D.W. van der Schaft, R.E. Seftor, E.A. Seftor, A.R. Hess, L.M. Gruman, D.A. Kirschmann, Y. Yokoyama, A.W. Griffioen, M.J. Hendrix, Effects of angiogenesis inhibitors on vascular network formation by human endothelial and melanoma cells, J. Natl. Cancer Inst. 96 (2004) 1473–1477.
[70] L.K. Dunn, K.S. Mohammad, P.G. Fournier, C.R. McKenna, H.W. Davis, M. Niewolna, X.H. Peng, J.M. Chirgwin, T.A. Guise, Hypoxia and TGF-beta drive breast cancer bone metastases through parallel signaling pathways in tumor cells and the bone microenvironment, PLoS One 4 (2009) e6896.
[71] A. Mohyeldin, T. Garzon-Muvdi, A. Quinones-Hinojosa, Oxygen in stem cell biology: a critical component of the stem cell niche, Cell Stem Cell 7 (2010) 150–161.
[72] E.B. Rankin, A.J. Giaccia, E. Schipani, A central role for hypoxic signaling in cartilage, bone, and hematopoiesis, Curr. Osteoporos. Rep. 9 (2011) 46–52.
[73] A.P. Kusumbe, R.H. Adams, Osteoclast progenitors promote bone vascularization and osteogenesis, Nat. Med. 20 (2014) 1238–1240.
[74] A.P. Kusumbe, S.K. Ramasamy, R.H. Adams, Coupling of angiogenesis and osteogenesis by a specific vessel subtype in bone, Nature 507 (2014) 323–328.
[75] K. Raymaekers, S. Stegen, N. van Gastel, G. Carmeliet, The vasculature: a vessel for bone metastasis, Bonekey Rep. 4 (2015) 742.
[76] V. Almendro, A. Marusyk, K. Polyak, Cellular heterogeneity and molecular evolution in cancer, Annu. Rev. Pathol. 8 (2016) 277–302.